Mon. Not. R. Astron. Soc. **270,** 21–34 (1994)

Resonance capture and the formation of the outer planets

C. Beaugé,[1] S. J. Aarseth[2] and S. Ferraz-Mello[1]

[1] *Instituto Astronômico e Geofísico, Universidade de São Paulo, Av. Miguel Stefano 4200, 04301-904 São Paulo, Brazil*
[2] *Institute of Astronomy, Madingley Road, Cambridge CB3 0HA*

Accepted 1994 March 18. Received 1994 March 17; in original form 1993 December 17

ABSTRACT

In this paper we study a possible process for the formation of the outer planets, in which resonance capture induces the accretion of the planetary cores near exterior mean-motion commensurabilities of existing bodies. A two-dimensional *N*-body simulation is performed to test this hypothesis in the case of Saturn. Initial conditions consist of a swarm of 1000 equal-mass planetesimals distributed over a planar ring with extrema at 6.5 and 15 au. All bodies are originally in circular orbits. For the dynamical evolution of the population, the following interactions are considered: mutual gravitation between the bodies, physical collisions, gravitational perturbations from an existing Jupiter (present mass and orbit) and gas drag. The simulation is followed until a single body remains. The results show a single planetary core in a stable orbit with elements $a = 9.78$ au and $e = 0.086$, well in accord with the present-day Saturn. We also discuss the possible extension of these results to the formation of the other major planets.

Key words: accretion, accretion discs – methods: numerical – celestial mechanics, stellar dynamics – planets and satellites: general – Solar system: formation.

1 INTRODUCTION

Of all the major members of our Solar system, the outer planets Jupiter, Saturn, Uranus and Neptune are the most controversial regarding their cosmogony. A particular problem is posed by their physical structure, which is characterized by large gaseous envelopes of quasi-solar composition surrounding solid cores of heavy elements, and places these bodies half-way between the terrestrial planets and the Sun. According to the basic assumptions for the formation process, current cosmogonic theories can be classified in two main categories: the so-called 'gas-instability' and 'core-instability' models.

In the first of these models (e.g. Cameron 1978), the solar nebula, after its contraction into a thin disc, became locally unstable in a manner analogous to a Jeans-type instability in which the gravitational energy of a gaseous sphere exceeds its thermal energy. As a consequence, the disc broke up into several contracting gaseous envelopes. Coalescence of these separate clouds ultimately produced four giant gaseous protoplanets. These condensations initially encompassed volumes several thousand times larger than the present planets, in accordance with the generally accepted low-density profile of the nebula. Subsequent hydrodynamical collapse of the envelopes, followed by slow contraction in quasi-hydrostatic equilibrium, led to the origin of the present planets. Throughout this process, the composition remained solar and homogeneous. In this model, two possible mechanisms are postulated in order to explain the formation of solid cores in the correct fractional mass range of 3–90 per cent, versus ~1 per cent for solar abundance. According to Cameron, DeCampli & Bodenheimer (1982), once the heavy elements accumulated at the centre of each envelope, a large fraction of the gas was lost owing either to tidal stripping by the forming Sun, or to thermal evaporation as the solar nebula's temperature increased. A different mechanism (Pollack, Burns & Tauber 1979) postulates that the gaseous envelopes may have gained cores through the gas drag capture of planetesimals from the surrounding solar nebula. Such a capture mechanism may have been particularly efficient at times soon after the protoplanets formed, when they were much larger than the present dimensions of the Jovian planets. Either way, the basis of this model is a formation mechanism similar to that of stellar objects, in which the dynamical evolution of the gas prevailed over the solid bodies of the primordial system.

The core-instability or nucleation model (see, for example, Mizuno 1980) is, in various senses, a mirror image of the one above. Here, the solid cores formed first through two-body accretion of the rocky planetesimals present in the disc. These cores grew to a certain critical mass and were then able to capture permanently a massive envelope from the surrounding solar nebula. This capture occurred not instantaneously, but in stages. Thus, during the first stage, each

core grew much more rapidly than the envelope. When the envelope mass became comparable to the core mass, however, the rate of envelope accretion increased substantially and exceeded, by a large factor, the growth rate of the core. If we define the 'critical' core mass as the value at which the two growth rates are equal, then calculations show that it has a value of the order of $15\,M_\oplus$, in good accord with the known core masses of the outer planets.

Which of these two theories is correct is still an open question. However, observational and theoretical evidence seems to support the core-instability model. An argument in its favour is its ability to predict consistently the absolute value of the core mass and its relative insensitivity to conditions in the solar nebula. Elemental abundance also favours this model: there is a strong indication that Jupiter and Saturn are enriched in nitrogen. Also, all four outer planets show a definite enhancement of carbon relative to solar abundance (Gautier & Owen 1983). Thus it seems that the outer planets are enriched in heavy elements with respect to solar composition, in contrast with the predictions of the gas-instability hypothesis. Lastly, some models of Uranus and Neptune (Hubbard & MacFarlane 1980) require a large proportion of ice in the composition of the cores; this also favours the nucleation theory. For these reasons we adopt this model for our present study.

The particular question that we wish to address in this paper has less to do with the physics or chemistry of the outer planets than with their dynamics. It is known that the Jovian planets lie close to low-order orbital resonances when considered as pairs. The orbits of Jupiter and Saturn lie near the 2/5 commensurability, Saturn and Uranus near the 1/3 and Uranus and Neptune very close to the 1/2 orbital resonance. Is this observed configuration just a matter of chance, or is it an inevitable consequence of the formation process itself? This question has led to many recurring controversies as to whether or not these relationships can be explained simply as statistical accidents (see Molchanov 1968; Backus 1969; Hénon 1969) since, given four real numbers, it is always possible to fulfil several commensurate relations to some degree of accuracy. Furthermore, even though the outer planets are close to low-number commensurability relations, they are not actually *in* resonance. This also questions the statistical significance of the observed resonant configurations. The principal reason for scepticism, however, is the fact that, until recently, it had not been demonstrated that mean-motion resonances could have influenced the formation sites of these bodies.

A possible answer to this question was proposed by Weidenschilling & Davis (1985) with their discovery of resonance trapping resulting from gas drag. This phenomenon can be summarized as follows: solid particles in the solar nebula follow Keplerian orbits, but the presence of gas causes their orbits to evolve. Both eccentricity and inclination are damped, but the most important effect is a secular decrease in the semimajor axis. Owing to the presence of a negative radial pressure gradient in the gas, the nebula rotates at slightly less than the Keplerian velocity (Adachi, Hayashi & Nakazawa 1976), causing the solid particles to experience a loss of energy and angular momentum, even when in a circular orbit. Under certain initial conditions, however, a resonance between the planetesimal and an already formed planet (or embryo) can counteract this orbital decay and 'trap' the particles in a stable resonant orbit, where the planet supplies the energy and momentum removed by the drag. An important characteristic was also found: capture occurs only in exterior resonances, never in interior ones.

Patterson (1987) developed further the cosmogonic implications of this process, suggesting that resonant trapping may have played a fundamental role in initating privileged formation sites for the planets. Thus Patterson imagined a scenario in which Jupiter formed first and influenced the accumulation of planetesimals at low-order exterior commensurabilities. The high density of planetesimals at these locations would then encourage accretional collisions, resulting in the final formation of a massive core at or near resonance.

The phenomenon of resonance trapping may therefore provide an answer to this problem and explain the near-commensurability configuration of the outer planets. Although a number of numerical simulations of planetary formation have been performed in the past (e.g. Wetherill & Stewart 1989, Aarseth, Lin & Palmer 1993 and references therein), however, little consideration has been given to the role of two-body mean-motion resonances within this framework. Perhaps the first to consider this case was Greenzweig (1993), who analysed the evolution of a swarm of particles due to gas drag in the vicinity of a single commensurability. Notwithstanding this fact, no results were presented as to the direct cosmogonic consequences of this phenomenon.

In order to model precisely this process, we have performed an *N*-body simulation of the evolution of a swarm of 1000 planetesimals under the following effects: gravitational perturbation of an existing Jupiter; mutual gravitational interactions between the bodies; gas drag of the Stokes type; and physical encounters between the members of the population. The goal of this work is to see whether the interplay between gravity, drag and collisions in the swarm can result in a single planetary core with dynamical characteristics similar to Saturn. It is hoped that this will provide information on the capacity of mean-motion resonances to influence the formation sites of the planets.

2 RESONANCE TRAPPING

In this section, we review the principal aspects of resonance trapping, starting from the formulation of the planar restricted three-body problem. Special emphasis is placed on the existence of stationary solutions, which may act as points of capture, and on the dynamical characteristics of these stable points. Finally, we will study the extension of these results to the case in hand, where the presence of a whole swarm of interacting bodies may affect the previously known results. The cosmogonic implications and problems to be solved will also be treated in this section.

2.1 Stokes drag

We assume that there are neither turbulent motions nor large-scale circulations in the solar nebula and that the gas is rotating in a circular motion around the Sun. We do suppose, however, a negative radial pressure gradient in the nebula and, accordingly, the angular velocity of the gas, ω_g, will differ slightly from the Keplerian angular velocity, ω_k, of a

solid body. For the plausible assumption that the gas temperature varies inversely with radius, the ratio of gas velocity to Keplerian velocity (denoted by $\alpha = \omega_g/\omega_k$) is independent of the position in the nebula (Adachi, Hayashi & Nakazawa 1976; Weidenschilling 1977). Typical nebular models predict $\alpha \geq 0.99$; we use $\alpha = 0.995$ throughout, in accordance with previous studies of resonance trapping.

The gas drag acceleration on a particle moving through a resisting medium can be expressed in different forms, depending on the shape, size and velocity of the particle, and also on the condition of the gas. In the case of a spherical body, the magnitude of the drag force (per unit mass) can be written as

$$Y = \frac{3C_D\rho_g}{8R\rho_p}\Delta v^2, \tag{1}$$

where ρ_p is the mass density of the particle, R its radius and Δv its velocity relative to the gas. The non-dimensional drag coefficient, C_D, is a function of two quantities: the Knudsen number K ($= l/R$, where l is the mean free path of the gas molecules) and the Reynolds number, R_e ($= 2\rho_g \Delta v R/\mu$, μ being the viscosity and ρ_g the density of the gas). In the case where $K < 1$ and $R_e < 10$, which corresponds to low values of the gas density, the coefficient C_D can be approximated by $C_D \simeq 24/R_e$. Then the drag force Y is given by Stokes' formula

$$Y \simeq \frac{9\mu}{2\rho_p R^2}\Delta v. \tag{2}$$

Thus Stokes drag is linearly proportional to the relative velocity and does not depend explicitly on the gas density. By writing Δv in terms of the velocities in the inertial frame and defining $C = 9\mu/2\rho_p R^2$ as the new drag coefficient, we obtain the final expression for the Stokes drag acceleration in vectorial form:

$$\boldsymbol{Y} = C(\dot{\boldsymbol{r}} - \alpha\boldsymbol{\omega}_k \times \boldsymbol{r}). \tag{3}$$

For $\rho_p = 3$ g cm^{-3} and a gas composed primarily of hydrogen molecules at temperature $T = 100$ K, we obtain

$$R^2 C = 11.1, \tag{4}$$

which gives the functional relationship between the radius of the planetesimal (in cm) and its corresponding drag coefficient (in d^{-1}).

2.2 The restricted problem

So far, studies of resonance trapping resulting from Stokes drag have been limited to an analysis of the planar restricted three-body problem (Sun, planet and massless particle). In this formulation, the elliptic orbit of the planet is considered fixed, while the osculating orbital elements of the massless body suffer temporal variations due to both the gravitational pull of the planet (expressed by the disturbing function F) and the effect of the gas drag. Let us suppose that the mean motions of both secondary bodies lie close to a generic $(p+q)/p$ mean-motion resonance. In other words, let the ratio between the orbital periods be

$$\frac{T_1}{T} \approx \frac{p+q}{p}, \tag{5}$$

where T, T_1 are, respectively, the orbital periods of the particle and the planet, and p and q are small integers. In this case, after averaging over the short-period terms, the Fourier expansion of the disturbing function F in terms of the elliptical elements of the bodies can be well approximated by a series of the type

$$F = \sum_{i,j=-\infty}^{\infty} A_{i,j}\cos(i\sigma + j\sigma_1), \tag{6}$$

where the coefficients $A_{i,j}$ are functions of the semimajor axes, a and a_1, the eccentricities, e and e_1, and the mass of the planet, m_1. The argument of this series expansion is given in terms of two angular variables (σ, σ_1) called *critical angles* of the resonance. They are defined in terms of the mean longitudes, λ and λ_1, and the longitudes of perihelion, ϖ and ϖ_1, as

$$\begin{aligned} q\sigma &= (p+q) - \lambda_1 - p\lambda - q\varpi, \\ q\sigma_1 &= (p+q)\lambda_1 - p\lambda - q\varpi_1. \end{aligned} \tag{7}$$

Because the effect of the dissipation force $\boldsymbol{Y}$ is a secular and simultaneous decrease in both the semimajor axis and eccentricity of the body, trapping will occur only when the gravitational contribution of the planet (given by $\mathrm{d}F/\mathrm{d}\boldsymbol{r}$) also involves a secular, but now simultaneous, increase in the same variables. Such a balance of forces was found to exist only when the body experiences an exterior commensurability relation with the perturber (Weidenschilling & Davis 1985). A recent paper by Beaugé & Ferraz-Mello (1993) determined the conditions for trapping, as well as the final stable orbits of these bodies. Their results can be summarized as follows.

(i) Given a generic exterior resonance $(p+q)/p$ (i.e. $p < 0$), trapping can occur for all bodies with radius $R \geq R_{min}$, where $R_{min} = R_{min}(p, q)$. The numerical value of this minimum radius decreases for resonances closer to the planet ($R_{min} \propto 1/a$). Therefore, as a general rule, larger bodies will be preferentially trapped at distant resonances, while smaller bodies will pass them and only suffer capture at points closer to the planet.

(ii) The capture mechanism is extremely sensitive to the initial conditions. Thus, a choice of initial orbital elements that place the particle outside a certain resonance and radius for which the commensurability allows capture does not guarantee that trapping will effectively take place. The particle may just pass through and finally be stopped at another resonance for which the value of R also allows capture.

(iii) The final orbits of the trapped planetesimals are of two types: σ-libration (i.e. Lindblad) and corotation. If the radius of the particle is larger than a certain value, R'_{min}, the final orbit will be a libration where the critical angle σ exhibits a small-amplitude oscillation (i.e. σ-libration) around a certain fixed value. In this type of solution, the other critical angle (σ_1) circulates freely taking all values from 0 to 2π. However, if $R_{min} < R < R'_{min}$, then the captured body will exhibit a simultaneous libration of both critical angles around fixed values. In asteroidal dynamics, this type of orbit is usually referred to as a corotation (Ferraz-Mello, Tsuchida & Klafke 1993). Table 1 shows the values of both minimum radii for some important resonances.

Table 1. Minimum radii for capture in corotation and libration, for various exterior resonances. Units are metres.

$(p+q)/p$	R_{min}	R'_{min}
3/4	2.20	5.15
2/3	3.18	6.09
1/2	7.27	15.72
1/3	26.36	39.86

Table 2. The universal capture value of the eccentricity for libration in exterior resonances. Semimajor axis is in units of a_1.

$(p+q)/p$	a	e	$a(1-e)$	$a(1+e)$
4/5	1.160	0.033	1.122	1.198
3/4	1.211	0.037	1.166	1.256
2/3	1.310	0.043	1.254	1.367
3/5	1.405	0.048	1.338	1.473
4/7	1.452	0.050	1.380	1.524
1/2	1.587	0.054	1.501	1.673
2/5	1.841	0.061	1.730	1.953
1/3	2.079	0.064	1.945	2.214
1/4	2.519	0.070	2.343	2.695

(iv) The main difference between the two types of solutions is the degree of accumulation, in real space, suffered by the trapped particles. For σ-libration orbits, accumulation occurs only in the radial component (i.e. semimajor axis), but not in the azimuthal angle, since σ_1 is not locked into the resonance. In corotations, however, the solutions correspond to coherent motions: a swarm of test bodies will move on the same ellipse and cluster about $|p|$ evenly spaced phases of the azimuthal angle. This coherence property is unique in non-collisional celestial mechanics.

(v) Another difference between capture in σ-libration and corotation, independent of the temporal behaviour of the resonance angular variables, is the equilibrium value of the eccentricity. In corotation, the final value of e depends on the equilibrium value of σ_1 and can be as low as ~ 0.03 or as high as ~ 0.12, while, in the case of σ-libration, the eccentricity is a fixed universal quantity, depending only on the particular resonance at which the capture takes place. This allows us to predict precisely the eccentricity that each captured body will have at every commensurability. Table 2 presents the calculated values of this universal eccentricity for various exterior resonances. Note that, as we look at commensurabilities closer to the planet, the value of e decreases. In the limiting case $|p| \to \infty$, corresponding to a 1/1 resonance with the planet, we have $e \to 0$.

(vi) Outside the resonance, the rate of the radial drift in the body's semimajor axis is given by

$$\frac{da}{dt} = -Ca[1-\alpha+O(e^2)]. \tag{8}$$

For small values of the eccentricity, the above equation may be integrated independently and yields the value of a as a function of time:

$$a(t) \simeq a_0 e^{-C(1-\alpha)t}, \tag{9}$$

where a_0 is the initial semimajor axis corresponding to $t=0$. We see from this expression that, since $\alpha < 1$, the body will suffer a monotonic decrease in energy even when in a circular orbit. Furthermore, this expression allows us to estimate the time it would take a certain body to reach a resonance and be captured. For example, for $R = 50$ m, the spiralling from $a_0 = 15$ au to the 2/5 resonance with Jupiter, situated at $a = 9.7$ au, takes approximately half a million years.

2.3 Extension to the *N*-body case

Before extending these results to the N-body case at hand, let us momentarily consider an intermediate step, which consists of replacing the third body studied in the subsection above by a swarm of massless planetesimals. Let us further suppose that all particles are assigned different drag coefficients, C_j, and have initial semimajor axes placing them in an extended ring outside the orbit of Jupiter. Accordingly, the evolution of each body will still follow the laws of the restricted three-body problem, and, because of the finite capture probability of each resonance and the range of C-values, the end result of the evolution will be a series of thin rings in which different proportions of the swarm are captured in different resonances. In each case, the orbits will display either σ-libration or corotational motions.

An example of this behaviour can be seen in Fig. 1. Here we show the temporal evolution, and capture, of 10 test particles (radii $r = 10$ m). Initial conditions are $a = 9.5$ au and $e = 0.01$, common to all bodies, although slightly different values of the mean longitude were adopted. In Fig. 1(a) we have plotted the variation of the semimajor axes as a function of time. After the initial monotonic decrease in energy, the bodies encounter their first important resonance, the 1/2 ($p = -2$, $q = 1$), situated at $a \simeq 8.3$ au. Capture does not take place at this commensurability, and the orbital decay continues until three particles are trapped in corotation by the 3/5 ($p = -5$, $q = 2$) resonance. The remaining bodies pass through, and are finally captured in a σ-libration orbit by the 2/3 ($p = -3$, $q = 1$) commensurability.

In Fig. 1(b) we show the positions of all ten bodies, in Cartesian heliocentric coordinates, corresponding to the orbital evolution of the previous graph. In other words, each of the points in Fig. 1(a) has been transformed to its position in real space and plotted. Thus, the orbital decay is now seen as a slow spiralling of the dots towards the central part of the figure (i.e. the Sun). Jupiter is represented by a full circle and its orbit (circular approximation) by a broken closed curve. As mentioned in the previous subsection, we can see that the bodies captured in the 3/5 resonance display a coherence in the resulting motion: five accumulation points in the phase. In contrast, the particles captured in the 2/3 commensurability do not show this type of behaviour, the dots filling a dense and closed curve in real space.

Let us now introduce a mass for each planetesimal and discuss its subsequent effect on the resonant configuration. Fundamentally, two new perturbations enter the scene: mutual gravitational interactions between the members of the swarm and collisions. At first sight, it is hard to predict

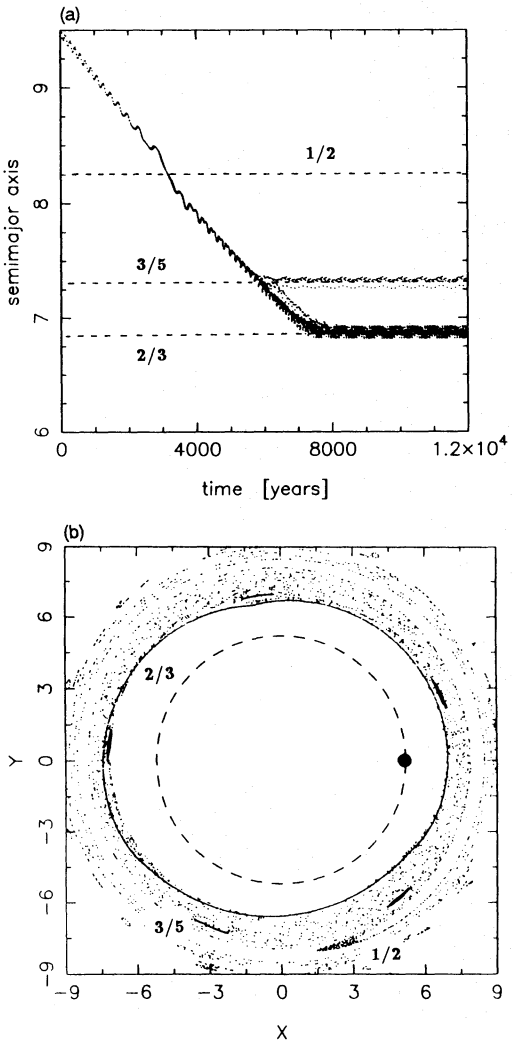

Figure 1 Numerical simulation of the evolution of 10 massless bodies and their posterior capture in two mean-motion resonances. (a) Evolution of the semimajor axes as functions of time. (b) Positions of the bodies (in heliocentric Cartesian coordinates) during the infall and posterior trapping. Note the differences in the behaviour of the azimuthal angle.

whether the interactions will promote the accretion of bodies. On one hand, the mutual attraction of particles at different resonances may induce an overlapping of the orbits and lead to accretional collisions; or they may even enlarge the commensurability's attractor basin, thereby increasing the capture probability of the resonance, making future trappings more likely. On the other hand, these same interactions, especially between bodies trapped at the same commensurability, may break the stability of the three-body solution, causing the individual particles to leave the resonance region and finally collide with Jupiter.

In the case of collisions, the most important effect to bear in mind is that, whatever the outcome, be it accretion or fragmentation, the result will be a change in the radius of the particle, and accordingly a modification of the drag coefficient the particle feels from the gas. The key question is then whether the new stable solution, corresponding to the new radius, will be sufficiently close to the previous one to allow the planetesimal to migrate towards it remaining trapped. If this is not the case, then each collision in the swarm will cause expulsion of the body from resonance and therefore the very basis of the present hypothesis would be untenable.

A different point was put forward by Weidenschilling & Davis (1985). They noted that planetesimals caught in neighbouring resonances (e.g. one trapped in the 2/3 and another trapped in the 3/5 commensurability) had forced eccentricities sufficiently high so as to cause an overlapping of their orbits. Thus the σ-libration orbits of bodies in different resonances would overlap, making collision between them possible. This property can be seen clearly in Fig. 1 for the above-mentioned resonances, and also in Table 2, where the fourth and fifth column show the perihelion and aphelion distance of libration orbits for different commensurabilities, respectively. We see that in most cases these orbits do in fact intersect, and therefore collisions between them are likely.

From all these considerations, it is clear that an immediate extension of the known mechanisms of resonance trapping to the N-body case is not possible. The relative importance and behaviour of these perturbations are, for the time being, unpredictable. The fundamental question that can be posed is whether these effects will be advantageous for the formation mechanism, and promote the formation of a single body in the neighbourhood of Saturn's orbit, or whether they will destroy the stability of the system and cause a general decay towards Jupiter. It is precisely this question that we hope to address with our simulation.

3 THE SIMULATION

For the present simulation, two numerical methods are feasible: a direct N-body code (e.g. Aarseth et al. 1993) or a Monte Carlo stochastic approach (e.g. Wetherill & Stewart 1989). The latter has the advantage of being able to handle a huge number of bodies (of the order of 10^6 or more), but at the cost of grossly approximating all gravitational and collisional interactions between them. In contrast, the former type of method is able to simulate the dynamical evolution of the swarm with relatively high precision, the accuracy of which depends fundamentally on the integrator in use, and not on any ad hoc simplifications and/or assumptions about these forces. The cost of such detailed treatment is, however, once again high, and N-body codes can rarely deal with populations of more than $\sim 10^3$ members. Thus, of the two main characteristics of the problem (i.e. initial conditions and interactions), the latter approach deals well with the first but not with the second, while the reverse holds for the former method. Which method to apply, then, depends on two aspects: first, which of the two characteristics is most important to the system; and, secondly, whether all the interactive forces of the problem can be modelled in a manner suitable for a Monte Carlo treatment. If the answer to this question is negative, no choice is available at all, and an N-body code must be used.

The first aspect is usually very subjective, and most of the time a reasonable answer is impossible without actually using both methods and comparing results. The second, however, is more concrete. Even though stochastic simulations can deal with mutual gravitational interactions and collisions, and have done so in the past (see Wetherill & Stewart 1989), the same is not true for the commensurate gravitational

forces intrinsic to the process of resonance trapping. At present, this phenomenon cannot be satisfactorily modelled in an analytic formulation and can only be treated by direct N-body simulations. The reasons for this can be summarized in the following manner. On one hand, no adequate analytical model exists to date for the exterior elliptic three-body problem, only the circular case having been recently mapped (Beaugé 1994). On the other hand, as was mentioned in the previous section, the mechanism of capture is probabilistic in nature. Since the dissipative system under consideration is not adiabatic (Beaugé & Ferraz-Mello 1993), and no analytic or semi-analytic theory for such systems is available, this process cannot be modelled either.

3.1 The integrator

The N-body code used in this simulation is similar to that by Beaugé & Aarseth (1990). It is based on a fourth-order polynomial expansion of the force function and individual time-steps for advancing the numerical solution (Aarseth 1985). In heliocentric coordinates, the equations of motion for each body can be written as

$$\frac{\mathrm{d}^2\boldsymbol{r}_i}{\mathrm{d}t^2} = -\frac{G(\mathrm{M}_\odot + m_i)}{|\boldsymbol{r}_i|^3}\,\boldsymbol{r}_i - G\sum_{\substack{j=1\\ j\neq i}}^{N} m_j\left(\frac{\boldsymbol{r}_i-\boldsymbol{r}_j}{|\boldsymbol{r}_i-\boldsymbol{r}_j|^3}+\frac{\boldsymbol{r}_j}{|\boldsymbol{r}_j|^3}\right) - C(\dot{\boldsymbol{r}}_i - \alpha\boldsymbol{\omega}_i\times\boldsymbol{r}_i), \qquad (10)$$

where G is the gravitational constant, $\mathrm{M}_\odot$ is the mass of the Sun and m_j is the mass of the jth particle. The last term in equation (10) represents the external dissipative force (per unit mass) due to the Stokes drag.

In order to reduce the time-consuming force calculations of all bodies, we employ a perturbation scheme based on nearest neighbours. The orbital plane is divided into 100 azimuthal and 18 radial zones. Each body is then assigned a particular grid-point, depending on its position. Usually, the perturber selection is based on a distance criterion (e.g. Lecar & Aarseth 1986). In this scheme, particle m_a acts as a perturber of m_b only if the grid-distance between two bodies is less than a certain value. The main drawback of this criterion is that there is no mass dependence. In other words, there is no distinction between m_a being a tiny fragment or a fully grown planet. If we implement a collision model with fragmentation as a possible outcome, then we should expect a large number of fragments in the population, with some having very small mass. It is therefore not necessary to include their perturbations out to large distances. On the other hand, since our planetary formation scenario is based on orbital resonance, it is important to allow growing embryos to influence other formation sites, and therefore their perturbations should extend quite far. With this in mind, the following perturber criterion is introduced: once a planetesimal's mass grows sufficiently for it to be qualified as a possible planetary embryo ($m_i > 10m_0$, with m_0 the initial mass), its gravitational perturbation is included on every other body of the swarm, independent of its bin location. For masses below the embryo limit, perturbations are considered only when the difference in bins (radial as well as azimuthal) is at most an integer n_i, defined as a function of mass by

$$n_i = 1 + 2\sqrt{m_i/m_0}\,. \qquad (11)$$

Perturbations on particles with grid-points outside this specific range are ignored. Finally, full N-body perturbations are included for all embryos throughout the simulation. For Jupiter, no approximation was employed, either in its gravitational effects on the whole swarm or for perturbations from these bodies on the planet itself.

The consequence of these modifications is that full perturbations are considered for all growing embryos throughout the simulation, and only for small bodies are the gravitational forces approximated. As a check of the precision of our N-body code, the semimajor axis of a single dissipationless particle under the gravitational field of the Sun, integrated over 10^6 yr, suffered a variation of less than 10^{-4} au.

3.2 Collision model

Since the aim of this paper is to study the formation of a planet through the agglomeration of an initial swarm of small bodies, we need a realistic model with which to simulate such physical encounters. The model chosen here is based primarily on Greenberg et al. (1978) and Spaute, Lago & Cazenare (1985), and we refer the reader to these papers for details. Let us suppose that a collision occurs between two planetesimals of total mass $M = m_1 + m_2$, with corresponding velocities $\boldsymbol{v}_1$ and $\boldsymbol{v}_2$. We then define the total impact energy due to the motion of the bodies relative to the centre of mass of the colliding pair by

$$E = \frac{1}{2}\frac{m_1 m_2}{m_1+m_2}\,V_\mathrm{r}^2\,, \qquad (12)$$

where $\boldsymbol{V}_\mathrm{r} = \boldsymbol{v}_2 - \boldsymbol{v}_1$ is the relative velocity. We also define the radial relative velocity, V_R, as the radial component of the vectorial relative velocity.

No collision between planetesimals is expected to be totally elastic, since some of the impact energy is dissipated as heat during the encounter. Denoting by η the fraction of E lost in this manner, the energy, E', after the collision is

$$E' = (1-\eta)E. \qquad (13)$$

Using equation (12), we define the radial rebound velocity

$$\boldsymbol{V}_\mathrm{reb} = -\sqrt{1-\eta}\;\boldsymbol{V}_\mathrm{R}, \qquad (14)$$

which is the radial velocity at which the bodies separate. The magnitude of η depends on the physical characteristics of the bodies. The value $\sqrt{1-\eta}$ is sometimes denoted by c_i and called the restitution coefficient, which can be thought of as the ratio between the rebound velocity and the impact velocity. In our case, we have chosen $c_i = 0.7$. We also define the maximum rebound velocity, V_c, as the greatest value of V_R at which a collision can occur with no damage to either body (crater formation or direct fragmentation). This parameter can be expressed in terms of the physical characteristics of the particles as

$$V_\mathrm{c} = \frac{2S}{c\rho}\,, \qquad (15)$$

where S is the impact strength, c the sound velocity and ρ the density of the body.

Depending on the magnitude of the radial impact velocity V_R, three different collision outcomes are expected: (i)

rebound; (ii) rebound with crater formation; and (iii) fragmentation. The first case, in which the post-collision bodies separate with no mass change, occurs when the rebound velocity is less than the maximum value ($V_{reb} < V_c$). Note that the velocity at which the bodies separate after the impact is affected by the coefficient of restitution. If this value is found to be smaller than the mutual escape velocity of the two-body system,

$$V_{esc} = \left[\frac{2G(m_1 + m_2)}{R_1 + R_2}\right]^{1/2}, \tag{16}$$

where R_i is the radius of a body, then the colliders are combined (accreted) into one body, using the centre of mass approximation.

If, on the other hand, $V_R > V_c$, but the impact is not so high as to shatter the bodies, then the structure is not strong enough to propagate the strain with sufficient speed, and the surface will suffer some local damage (crater formation), after which the bodies will separate at some fraction of their impact velocity. The cratering process has two consequences: first, it removes a certain amount of mass from each body; secondly, the ratio of rebound velocity to impact velocity is smaller than in the normal rebound ($V_{reb}/V_R = 0.5$), because of the additional loss of energy in cratering and mass ejection at the impact site. Both these aspects of the cratering process have been modelled following the bibliography cited above.

Finally, if the impact energy E is sufficiently high, the internal structure of the body cannot resist the impact and shatters. This occurs when the impact energy per unit volume (E/W) exceeds the impact strength of the body, S. Therefore, the body will shatter if

$$E > S_i W_i, \tag{17}$$

where S_i and W_i are the impact strength and volume of m_i ($i = 1, 2$), respectively. Consequently, one or both planetesimals will fragment. The resulting mass distribution and velocity dispersion of the fragments have been modelled following Beaugé & Aarseth (1990). One aspect of this model that should be mentioned specifically, however, is the existence of a minimum fragment size. This limit was set to $10^{-2} m_0$. A potentially catastrophic physical encounter involving such a body was simply ignored and treated as a rebound. The reason behind this lower bound is twofold. First, since the magnitudes of peculiar velocities are usually inversely proportional to the particles' size, fragments display a tendency to undergo further fragmentation and, consequently, a rapid increase in number. Unless a conservative limit is set to this 'breeding', not only would we spend most of the time following debris around the Sun, but the CPU time would become prohibitive. Secondly, our interest in the mass spectrum of the population is only in so far as it is significant for the dynamical influence of the formation site of the planetary core. The importance of particles smaller than this limit is minimal.

3.3 Initial conditions

We started with an initial population of 1000 bodies in circular orbits, having semimajor axes beween 6.5 and 15 au and a constant surface density distribution. Both limits of the ring were chosen so as to include the main region between Jupiter (5.2 au) and Uranus (19.2 au). The azimuthal angle of each particle was chosen randomly in the interval $[0, 2\pi]$. Our system was two-dimensional, so all bodies (as well as Jupiter) were confined to the plane. Their density was taken equal to $\rho = 2$ g cm^{-3}. Of all the model parameters, two that deserve special attention are the adopted values of the planetesimals' mass and radius. According to present-day knowledge, it is believed that the initial rocky population in this region may have been composed of as many as 10^{13} particles with radii in the range 10^2–10^4 m. Because such a large number of bodies cannot be studied in an N-body code, some type of simplification is therefore inevitable.

In this respect, it is important to bear in mind that forces of two different natures are considered in the present study: those proportional to the particles' mass (gravitational interactions and collisions) and those dependent on the bodies' radius (gas drag). Any simplification introduced into the parameters by the fact that we can only consider 1000 particles must therefore take this into account. For the gravitational forces, it is fundamental to assign a mass to each initial body such that the mass of the swarm equals that of the Saturn core. Only thus will we be able to reproduce the dynamical effects on the population due to the conservative forces. Consequently, the chosen initial value of each planetesimal's mass was 1/1000 of 15 $M_\oplus$. Similarly, the collisions were treated as if the particle radius was proportional to the cube root of this mass. For the gas drag, however, we have to assign a radius for each body that reproduces the dissipative effect of the original planetesimals (i.e. 10^2–10^4 m), and not that of the simulated swarm. This has an unfortunate consequence, in the sense that the adopted values of these two physical parameters are not consistent with each other. What is important, however, is that they allow us to reproduce the complete dynamical interactions in a manner consistent with the real population we are trying to simulate. The drag coefficient of the initial bodies was then set to a corresponding radius of 50 m, although this value was later modified when the planetesimals' size changed through collisions. Although this corresponding radius is smaller than the values expressed above, this allowed the planetesimals to feel a dissipation that was significant, thereby reducing the CPU time. Even so, the simulation described here took over 240 h on a 20-Mflop machine. Moreover, since we are only interested in the relationship between the population evolution and mean-motion resonances and not with formation times, the principal point to which we must pay attention is to ensure that the chosen dimension of the bodies allows capture in the main resonances. The value adopted here (see Table 1) is the smallest radius that guarantees this.

Finally, for Jupiter we adopted the present mass, radius and orbital elements (a and e).

4 RESULTS

The simulation was continued until a single body remained, which accumulated most of the initial mass distribution of the swarm. This occurred after 6.7×10^6 yr. The orbital stability of the final body was checked by integrating its motion for a further one million years and studying the evolution of the eccentricity. In this interval, no secular varia-

tion was found and we therefore consider the configuration to be stable over a significant length of time. The main results of the simulation are summarized in three sets of histograms, shown in Figs 2 and 3, which, read vertically, contain the evolution of some characteristic quantities. The set of histograms on the left [i.e. $M(a)$] shows the mass distribution of the swarm according to semimajor axis. Thus, bar n gives the total mass (in units of m_0) of bodies with semimajor axis in the interval $(a_n-0.25,\ a_n+0.25)$. Initially, the mass distribution follows a constant surface density law, therefore the population in each interval grows in proportion to a^2. The distribution evolves as the simulation proceeds, until at the end of the run a single body remains with a total mass of $877m_0$. The middle set of histograms, $N(e)$, shows the *number* distribution of bodies according to their heliocentric eccentricity, also as a function of time. In this case, each bar gives the number of bodies (not mass) with eccentricity in the range $(e_n-0.0025,\ e_n+0.0025)$. Since the histogram is truncated at a maximum value of 0.08, all bodies with eccentricities beyond this value are summed in the last bar. Finally, the set on the right, $C(a)$, shows the distribution of collision sites in terms of the semimajor axis, as a function of time. Bar n at time t_i gives the number of collisions that have occurred in the interval $t\in(t_{i-1},\ t_i)$ for bodies with semimajor axis $a\in(a_n-0.25,\ a_n+0.25)$. This histogram gives valuable information about the frequency and location of the accretion process in the swarm. Figs 2–9 allow us to study the formation process of the final body.

The dynamical evolution of the swarm, from its initial homogeneous configuration until its final planetary core, can be divided into three distinct stages. Physically, they can be defined in the following way: an initial stage, in which the first small-size planetary embryos ($20m_0 > m > 10m_0$) form out of the original equal-mass distribution; a second stage, where the growth of the embryos is sufficiently advanced to allow significant gravitational interaction between them; and a final stage, in which a small number of large embryos dominate the system and finally accrete to form the planetary core. Each of these phases, which at first glance may seem arbitrary, is accompanied by a significant change in the dynamical evolution of the system and, particularly, in the role of each process governing the evolution. Let us recall that four distinct interactions have been included in our model: gas drag, mutual gravity between swarm members, gravitational

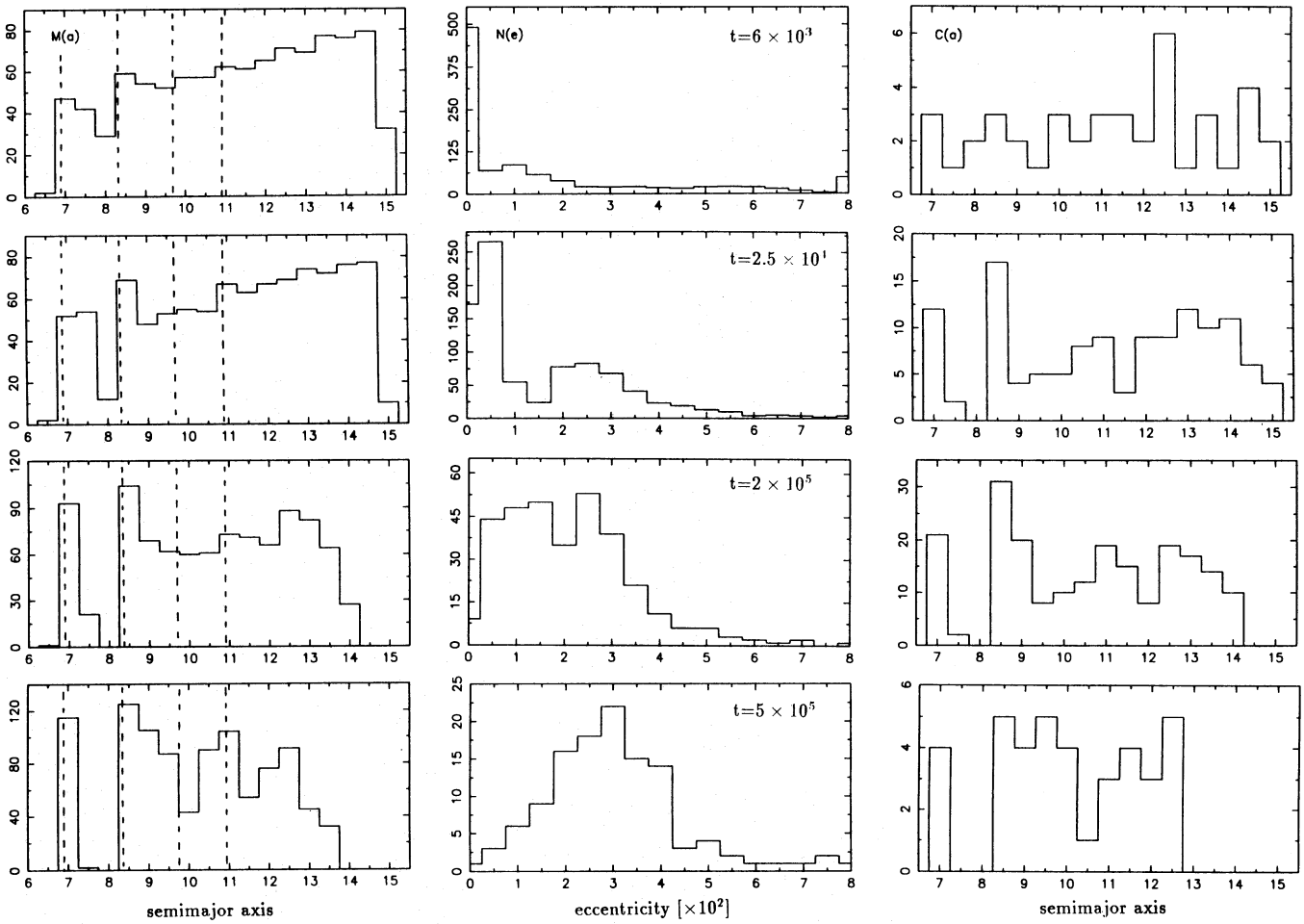

Figure 2. First stage of core formation. The column of histograms on the left [$M(a)$] shows the temporal evolution of the mass distribution according to semimajor axis. The middle column [$N(e)$] shows the number distribution according to eccentricity. The column on the right [$C(a)$] indicates the collision sites. Note the semimajor axes of the main resonances (here in broken lines): $a_{2/3}=6.8$, $a_{1/2}=8.3$, $a_{2/5}=9.7$ and $a_{1/3}=10.8$, in au. See text for details.

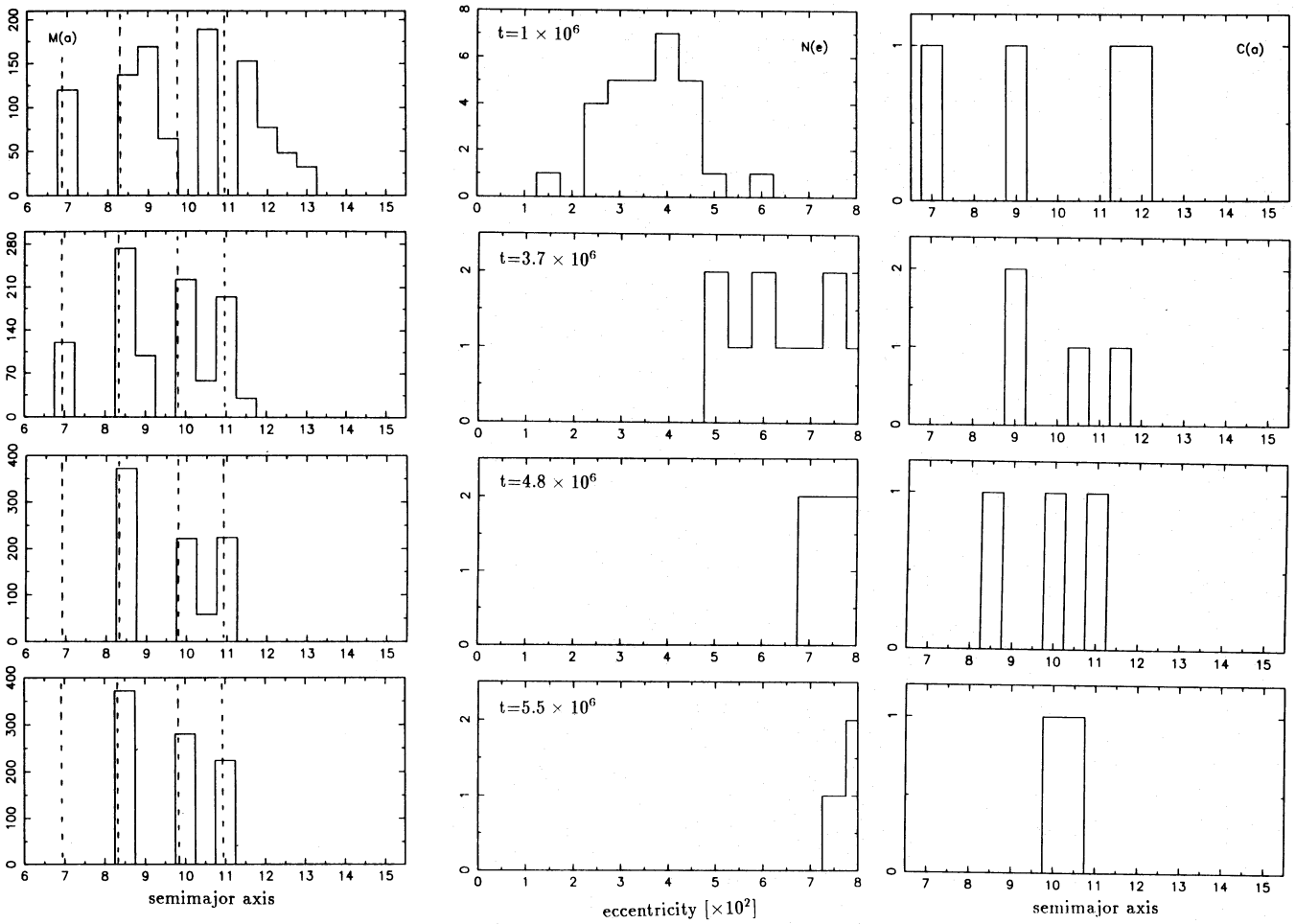

Figure 3. As Fig. 2, but for the second stage of formation.

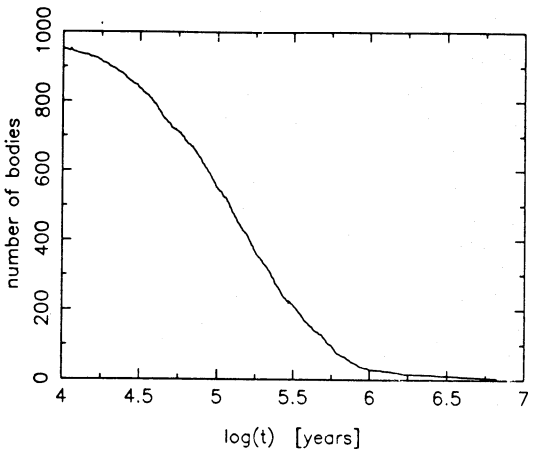

Figure 4. Number of bodies in the swarm as a function of time. During the second stage, the population decreases almost logarithmically with time.

perturbations of Jupiter (whether resonant or secular) and physical collisions. As we shall see below, the relative importance of each interaction varies during the simulation. For example, the role of resonance trapping decreases as the mutual gravitational interactions grow larger which, in turn, depends on the size of the embryos. Thus, each stage marks not only a specific characteristic of the mass spectrum of the population, but also a particular dynamical process at work.

4.1 Embryo formation

The first identified stage, referred to as the 'embryo-formation' stage, extends up to approximately 5×10^5 yr of the simulation. Its principal macroscopic characteristic is a marked regularity in the evolution of the system, as regards both the dynamics and collisions. Of the three forces present in the model, the mutual gravitational interactions are the least important. Since no significant single large mass (i.e. embryo) is as yet present to introduce a long-range coherent periodic perturbation, their main effect is reduced to a stirring of the peculiar velocities of the bodies, which implies small-amplitude oscillations both in semimajor axes and in eccentricities. In this sense, the orbital changes introduced are similar to those originating from the secular Jovian disturbing function, which dominates Jupiter's perturbation for bodies outside the major resonances. In the case of the eccentricities, however, close encounters between members of the swarm can yield moderately high values, as can be seen in Fig. 2 where, after 6000 yr, 48 particles have $e \geq 0.08$. These large values, which may in part be due to the

artificially large masses of the planetesimals, are nevertheless quickly damped by the gas drag, which tends to circularize the orbits, and, after 25 000 yr, only four bodies remain with eccentricities of this order. Because of the opposing effects of gravitational stirring and drag, the eccentricity for most of the planetesimals reaches an equilibrium value not larger than ~ 0.02.

The effect of gas drag, however, is fundamentally different. In this case, the orbital changes are not periodic but monotonic in nature. The orbital energy diminishes, thereby introducing a secular decrease in the semimajor axes of all bodies. Since the above-mentioned gravitational effects are incapable of counterbalancing this orbital decay, the whole population starts to spiral towards the Sun (see Fig. 2) at a rate proportional to the orbital radius. Owing to the combined effect of finite eccentricities and differential decrease in semimajor axes, the orbits of the bodies begin to intersect. The low relative velocity between particles enhances the probability of collisions and ensures that all such encounters end in agglomeration. Thus, after 400 yr, the first collisions occur in the population. These accreted bodies now have a smaller drag coefficient than the rest of the swarm and their orbital decay is therefore slower. This favours more orbital intersection with other bodies and further collisions. After a few thousand years, the original homogeneous mass distribution evolves towards a mass spectrum, with a few relatively large bodies ($m \sim 3m_0$) but with most of the mass still in the original range.

The orbital decay of each particle continues until it reaches a commensurability sufficiently strong for the resonant disturbing function to be comparable to the drag. Trapping becomes possible at this point. Owing to the sensitivity of the trapping mechanism to initial conditions, however, trapping may not necessarily take place at the first such resonance each body encounters. The body may well continue its orbital decay until it reaches another strong resonance, where the process repeats itself until finally a point is reached where conditions for equilibrium are favourable. The existence of such conditions is closely related to the overall efficiency of the trapping mechanism (Beaugé & Ferraz-Mello 1993) and this guarantees that capture will practically always occur at some commensurability.

Resonance trapping dominates the dynamical evolution of the inner half of the population during this first stage of formation. As each body is captured, its orbit migrates towards a stable stationary solution (σ-libration or corotation) and its eccentricity is excited to a value which, depending on the resonance and the type of solution, lies in the range ~ 0.04–0.06. Slowly, the original homogeneous distribution begins to show a series of rings of higher mass density, each corresponding to a different commensurability. During the first stage, collisions occur almost exclusively between pre-trapped bodies in the external part of the ring. This is caused by the fact that, for bodies with overlapping orbits, the probability of physical encounters is inversely proportional to the eccentricity. Thus, bodies outside the resonance zone (low eccentricity) have a greater chance of collisions than those captured in resonance, which display moderate pumped eccentricities. Nevertheless, as the population at each commensurability increases because of further trappings, collisions begin to occur at these points as well. At first, resonant collisions are noted primarily in small bodies trapped in corotation centres, as the phase-lock of the angular variables (see Section 2.2) also brings about an accumulation in real space. As the accreted (higher mass) planetesimals evolve towards libration orbits, however, physical encounters are observed also in these solutions.

It may seem plausible that corotation centres play an important role in the formation of embryos due to their higher collision probability with respect to σ-librations. However, this has not been the case. Since only bodies with radii $R < 40$ m can in fact be trapped in these points, this mechanism is effective only in the case of fragments. Consequently, it is possible that corotational trapping may be significant in limiting the breeding of small bodies, since these would tend to accumulate and accrete at these configurations. However, this hypothesis has not been checked.

Another interesting phenomenon can be seen after $\sim 3 \times 10^4$ yr. As more particles are trapped at each resonance, the corresponding capture probability increases. This occurs because, for an external body to pass through, it must now not only escape the capture mechanism of the resonance itself, but also escape collision with the growing ring of particles at that position. This enhanced trapping mechanism increases by a kind of feed-back effect: each capture increases the probability that the next body in line will be captured as well. The final effect is that the capture probability approaches unity at the larger commensurabilities. The first evident consequence of this phenomenon is the formation of 'gaps' between the rings of higher population density. After 50 000 yr one gap is clearly visible, lying between the 3/5 and 1/2 resonances. The combined probability of all resonances external to 1/2 is now unity and no further bodies spiralling down avoid capture at one of these points. The innermost section of the initial distribution ($a < 8$ au) is now disconnected from the main part.

From this time until the end of the first stage, the capture phenomenon starts to become polarized. Until now most resonances, up to third order, have contributed to the trapping of planetesimals, each in proportion to its strength. Soon, however, a significant number of particles accumulate at adjacent resonances so as to affect the stability of the weaker (higher order) commensurabilities. As a consequence, the stability of the 3/7, 3/5 and 4/7 exterior resonance points is destroyed and the few particles present there evolve and migrate towards other, stronger resonances. In particular, the 2/3, 1/2 and 1/3 commensurabilities accelerate their growth, either by capturing bodies spiralling from the outer half of the ring or by cannibalizing neighbouring resonances. A second gap begins to form around $a \simeq 7.3$ au as the bodies trapped at the 3/5 resonance evolve towards the 2/3 resonance. The number of embryos in the population grows at an increasing rate (Fig. 5) until a total of 34 large bodies are present in the swarm, almost all in librating orbits around mean-motion commensurabilities. However, no runaway growth is yet observed in the population. Most of the embryos have similar masses (~ 12–$16m_0$) and there is no evident tendency for one (or a few) of them to monopolize the accretion process and create a runaway situation. The great majority of the particles still lie in the original mass range (Figs 5 and 6).

This marks the end of the first stage of the simulation. The original distribution of bodies, which ranged from 6.5 to 15 au, has now evolved into two separate parts: an inner

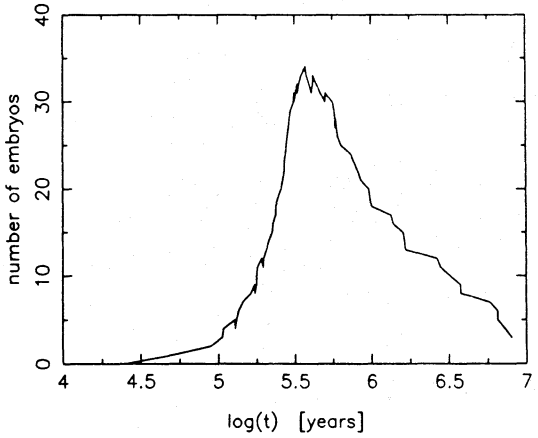

Figure 5. Number of embryos ($m > 10m_0$) as function of time. During the second stage, the number increases substantially due to the radial motion brought about by the predominant gravitational interactions of the swarm. The maximum value of the number of embryos is 34. In the third and final stage, these bodies accrete, their number diminishing until only a single particle remains.

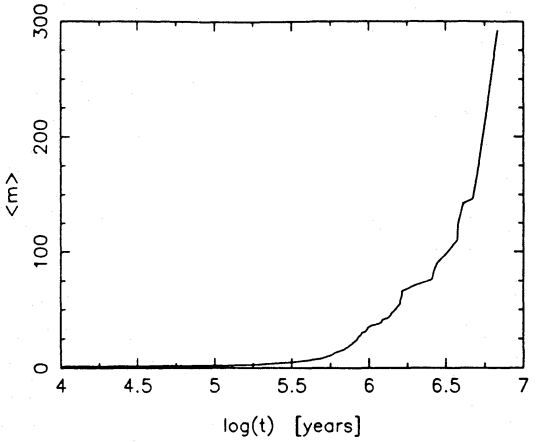

Figure 6. Mean mass of the population as a function of time.

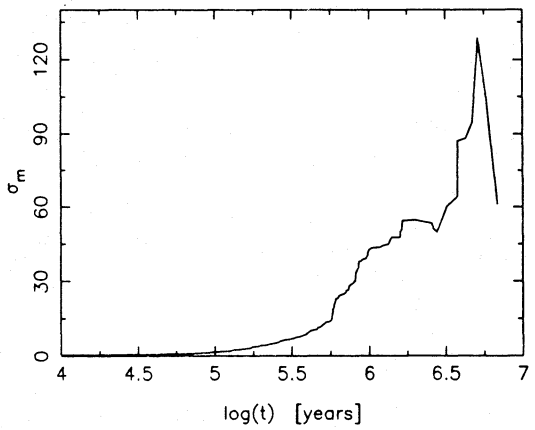

Figure 7. Mass dispersion of the swarm as a function of time.

ring, where all material with initial semimajor axis smaller than ~8 au has concentrated at the 2/3 resonance, and an independent main ring which now extends from 8.2 to 14 au. In this latter case, three resonances (1/2, 2/5 and 1/3) compete for dominance.

4.2 Embryo interaction

After approximately 5×10^5 yr, the growth in the population of each major resonance has reached a critical stage. Until now, collisions at these points have occurred principally between trapped bodies and external particles with almost circular orbits. Physical encounters between particles at resonance have been rare due to the larger eccentricity of these bodies. Now, however, as the number of small bodies and embryos grows in the commensurability regions, the probability of collisions increases in these domains. This brings about a substantial growth in the mass of the resonant embryos (Fig. 6) and these bodies begin to perturb significantly the stability of the captured bodies. This process feeds on itself rapidly, and a significant runaway growth starts to occur in the swarm (Fig. 7). The gravitational interactions from the fast growing embryos start to compete with the resonant perturbations from Jupiter, and a significant amount of radial mixing occurs in the population. Interchanges in orbital energy between particles makes their semimajor axes display irregular variations in time and the eccentricity increases beyond the equilibrium value (Fig. 3 at $t = 3.7 \times 10^6$ yr).

Coalescence between embryos themselves increases this effect until the mutual gravitational interactions are so large that they destroy the stability of most major resonances. Only the 2/3 commensurability continues to survive, owing to its great distance from the rest of the swarm. In all others, however, the particles no longer exhibit σ-libration or corotational motion and their dynamical evolution once again depends solely on secular interactions and gas drag. This expulsion from the stability of resonance trapping has dynamical consequences that are mass-dependent. Large embryos, with very low drag coefficients, suffer almost no perceptible orbital decay and, even though their semimajor axes exhibit irregular behaviour due to perturbations from other embryos, there is little trace of a secular decrease. Low-mass bodies, however, start once again to 'feel' the drag significantly. Their eccentricities are damped and their semimajor axes begin to decay, greatly increasing the probability of agglomeration of small bodies. As a consequence of this enhancement of collisions of small bodies (but not of larger ones), the mass dispersion of the distribution σ_m stabilizes and actually decreases during a certain interval of time [see Fig. 7 at $\log(t) \simeq 6.2$].

As a result of this effect, the main portion of the swarm, which extends from 8.0 to 12.2 au at $t = 3 \times 10^6$ yr, starts to develop further gaps and subdivides into three rings. These are located approximately at 8.5, 9.7 and 11 au, and correspond to those groups of planetesimals and embryos previously captured at the 1/2, 2/5 and 1/3 mean-motion resonances, respectively. A fourth solitary ring, associated with the 2/3 commensurability, is still observed at $a = 6.8$ au. These bodies, which until now have not participated in the chaotic stage because of their distance from the main population, are the last remnants of resonance trapping. Their orbits still exhibit σ-libration motions, which allow them to escape close encounters with Jupiter.

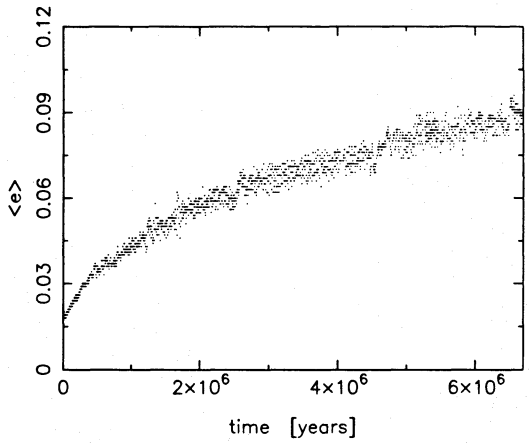

Figure 8. Mean eccentricity of the swarm population as a function of time.

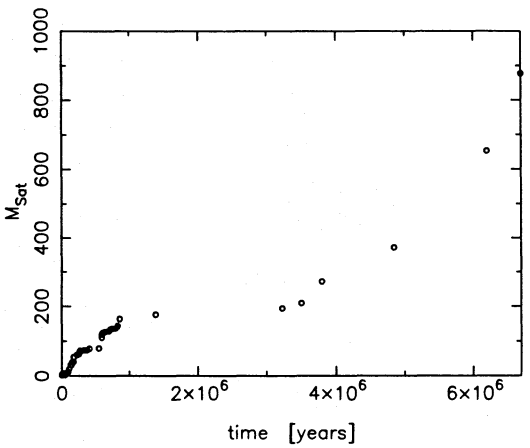

Figure 9. Mass of 'Saturn' as a function of time.

During the final epoch of this second stage of core formation, collisions diminish the number of bodies until only large protoplanetary embryos remain in each ring. Owing to the increase in relative velocities that has accompanied this stage (Fig. 8), a significant increase occurs in fragmentations and craterings; however, in the majority of cases the outcome is still accretion. The inner ring finally begins to be significantly perturbed by the main embryos; the stability of the 2/3 resonance breaks up and the body, of total mass $120m_0$, collides with Jupiter.

4.3 Embryo accretion

The last stage of planetary formation, about 5×10^6 yr from the beginning of the simulation, differs from the previous one by its simplicity. In each of the three remaining rings, all material has accreted in a single body. Thus, from the original population of 1000 planetesimals, only three remain. Their masses and orbital characteristics are

$$\begin{aligned} M_1 &= 372 \qquad a_1 = 8.73 \qquad e_1 = 0.076, \\ M_2 &= 283 \qquad a_2 = 10.03 \qquad e_2 = 0.083, \\ M_3 &= 224 \qquad a_3 = 10.91 \qquad e_3 = 0.111, \end{aligned} \tag{18}$$

where the masses are in units of m_0 and the semimajor axes are in au. Note that, although M_3 still lies in the vicinity of a resonance (1/3), this is not the case for the other two, where the gravitational perturbations have resulted in a significant migration from the original commensurability region.

In the final act, these three bodies collide, agglomerate and form the single planetary core of a Saturn-like planet. This occurred approximately 6.7×10^6 yr after the start of the simulation. The orbital elements of the surviving body are

$$a_s = 9.78, \qquad e_s = 0.086, \tag{19}$$

which show a remarkable similarity with the values of Saturn ($a = 9.52$ and $e = 0.062$).

5 CONCLUSIONS

The purpose of this paper has been to study the joint influence of mean-motion resonances and resonance trapping in the formation process of the outer planets. We have investigated a model composed of the Sun, an existing Jupiter and a planar extended ring of planetesimals embedded in the primordial solar nebula. By including the combined effects of gravitational perturbations, gas drag and resonance, we have simulated the formation of a Saturn-like core and obtained some insight into the role resonance trapping could have played in enhancing planetary formation at exterior resonance sites with Jupiter.

The results of our simulation are very encouraging. Not only did the original 1000-body planetesimal swarm accrete into a single planetary core, but the orbital characteristics of the final body resemble the real Saturn. We therefore conclude that the formation mechanism proposed by Patterson (1987) is plausible and may well explain the quasi-resonant configuration of the actual outer planets. It should be noted that, even though the formation process is related to the dynamical and evolutionary effects of mean-motion resonances, the final body *does not* lie in resonance with Jupiter. This is due to the fact that at no moment of the simulation did any particular commensurability dominate the rest and control the accretion and dynamics of the system. Rather, there was a rivalry between three different resonances, with similar populations. The mutual gravitational perturbations that led to collisions and agglomerations of captured bodies finally determined the formation site of the final core. Thus, the orbit of the Saturn-like core can be said to depend fundamentally on the capture efficiency and relative populations of the 1/2, 2/5 and 1/3 Jovian mean-motion resonances. Since in all three rings the captured mass was of the same order, the final body accreted at a value somewhere in between.

This result, in which mean-motion commensurabilities influence but do not determine the final configuration of the planet, may provide a possible explanation for the two peculiarities of Saturn's semimajor axis: namely, why did the resonance mechanism favour a resonance of secondary importance (2/5) in contrast to stronger neighbouring commensurabilities such as 1/2 or 1/3; and, secondly, if the formation site of Saturn is really due to resonance, why does the planet not lie precisely *at* commensurability with the perturber?

In order to investigate the differential role of each resonance, we performed a second simulation, analogous to the one described above, only this time the particles' initial drag coefficient was set at twice the previous magnitude. This value was chosen in such a way as still to allow capture in the 1/2 resonance and those closer to the perturber, but too small for the same outcome to occur in the 2/5 and 1/3 commensurabilities. In this way, we hoped to test the final outcome for less appropriate initial conditions. Results of this second simulation show great similarities with those presented above. Owing to the large number of two-body collisions in the outer ring prior to capture, some bodies arrived at the 1/3 resonance with dimensions sufficiently large to allow capture. A ring, formed by trapped planetesimals in libration orbits, originated at this point, helping to capture smaller particles. Collisions in resonance sites later resulted in a single large protoplanet at the 1/3 resonance. Similar behaviour was noted at the 1/2 resonance, but not in the 2/5 commensurability, in contrast to the previous simulation. Hardly any capture was observed in this region. The explanation for this effect can be found in the following: since the initial population has dimensions that are too small for capture at this point, trapping is only possible of bodies that have suffered collisions while still at the exterior portion of the disc. These particles, however, must pass through the 1/3 resonance before encountering the 2/5 one, and most of them will be trapped at the former point. Consequently, very few (if any) planetesimals will be effectively trapped in this latter commensurability. The cosmogonic implication of this behaviour is that the final Saturnian core formed at ~9.9 au, much closer to the 1/3 resonance than in the first simulation, but still close to the real Saturn.

A word of caution, however, is necessary. Even though most model parameters and interacting forces considered in this paper have been simulated with some realism, we must bear in mind that at least one such aspect is not completely consistent with current theories. We refer to the initial body size. Although we believe that our principal results are not very sensitive to this parameter, as can be seen by comparing the main simulation with the one described in the previous paragraph, the real test would be to increase the particle radius and not to decrease it. The required increase in CPU time, however, would make such a modification very expensive. One characteristic of our results, which should in fact vary according to the initial condition, is the formation time of the planetary core, especially the first stage (Section 4.1) which is the only one where the magnitude of the dissipation is truly important and, therefore, where the particle size is influential for the time-scale of the system. The last two stages, however, are more dependent on the planetesimal's mass and not on the radius, and so should be relatively unchanged.

With respect to the existence of runaway accretion during the accretion process, no sign of this effect was noted during the first stage of formation. Only in the second stage, once each strong resonance had captured a large amount of material in its vicinity, was some runaway observed.

As a final note, it is interesting that the three main resonances that have governed the formation process here are precisely those that are presently observed in the outer Solar system. As was shown at the beginning of this paper, Uranus lies close to the 1/3 commensurability with Saturn; and Neptune is situated near the 1/2 commensurability with Uranus. The inevitable question is then whether the same procedure could also account for the formation sites of these other Jovian planets. According to the model developed in this paper, once the Saturnian core captured a massive gaseous envelope from the surrounding nebula and acquired its present mass, it would in turn begin to affect the planetesimals present in the orbital feeding zone of these planets. Even though it is not prudent to extrapolate the present results, we may expect that the dynamical and collisional evolutions of the populations of these regions would follow approximately similar routes. If this were the case, then the final outcome of the formation process in the Uranus (Neptune) zone would be, once again, three large preplanetary cores near the 1/2, 2/5 and 1/3 mean-motion resonances with Saturn (Uranus). Now, if for some reason (e.g. external perturbations of Jupiter or smaller particle radii) the relative captured populations of these regions were different from those found in the present simulation, then the final planetary embryo would form closer to the 1/2 or 1/3 commensurability, as is the case with the actual planets.

Whether this last consideration applies, or is just an erroneous extrapolation, is a question that can only be answered by further studies. We emphasize, however, that the basis for the proposed model is very simple: aggregation of the initial distribution of planetesimals into the three strongest commensurabilities in the region and the subsequent accretion of their populations as soon as their mutual gravitational interactions surpass the stabilizing resonant perturbation of the mother planet. This mechanism has the advantage of being very robust relative to initial conditions such as the surface density of the swarm, total mass of the system and collision parameters, since resonances and resonance trapping will occur independently of them. We may therefore conclude that the formation of all the outer planets by this model is plausible.

ACKNOWLEDGMENT

This work was supported by the São Paulo State Science Foundation (FAPESP).

REFERENCES

Aarseth S. J., 1985, in Brackbill J. U., Cohen B. I., eds, Multiple Time Scales. Academic Press, New York, p. 377
Aarseth S. J., Lin D. N. C., Palmer P. L., ApJ, 403, 351
Adachi I., Hayashi C., Nakazawa K., 1976, Prog. Theor. Phys., 56, 1756
Backus G. E., 1969, Icarus, 11, 88
Beaugé C., 1994, Celest. Mech. Dyn. Astron., in press
Beaugé C., Aarseth S. J., 1990, MNRAS, 245, 30
Beaugé C., Ferraz-Mello S., 1993, Icarus, 103, 301
Cameron A. G. W., 1978, in Dermott S. F., ed., Protostars and Planets. Wiley, New York, p. 453
Cameron A. G. W., DeCampli W. M., Bodenheimer P. H., 1982, Icarus, 52, 1
Dermott S. F., 1968, MNRAS, 141, 363
Gautier D., Owen T., 1983, Nat, 304, 691
Greenberg R., Wacker J. F., Hartmann W. K., Chapman C. R., 1978, Icarus, 35, 1
Greenzweig Y., 1993, BAAS, 24, 984
Hénon M., 1969, Icarus, 11, 93
Hubbard W. B., MacFarlane J. J., 1980, J. Geophys. Res., 85, 225

Lecar M., Aarseth S. J., 1986, ApJ, 305, 564
Mizuno H., 1980, Prog. Theor. Phys., 64, 544
Molchanov A. M., 1968, Icarus, 8, 203
Patterson C. W., 1987, Icarus, 70, 319
Pollack J. B., Burns J. A., Tauber M. E., 1979, Icarus, 37, 587
Spaute D., Lago B., Cazenave A., 1985, Icarus, 64, 139
Weidenschilling S. J., 1977, MNRAS, 180, 56
Weidenschilling S. J., Davis D. R., 1985, Icarus, 62, 16
Wetherill G. W., Stewart G. R., 1989, Icarus, 77, 330